Femtoscopy analysis of ultrasoft pion trap at energies available at the CERN Large Hadron Collider

W. Rzesa,[1] G. Kornakov,[1] A. R. Kisiel,[1] Yu. M. Sinyukov,[1,2] and V. M. Shapoval[2]
[1]*Warsaw University of Technology, Faculty of Physics, ul. Koszykowa 75, 00-662 Warsaw, Poland*
[2]*Bogolyubov Institute for Theoretical Physics, 14b Metrolohichna Street, Kyiv 03143, Ukraine*

(Received 7 March 2024; revised 20 June 2024; accepted 31 July 2024; published 6 September 2024)

Femtoscopy studies of pion radiation in heavy-ion collisions have been conducted extensively at all available collider energies, both theoretically and experimentally. In all these studies special attention is given to m_T dependency of pion femtoscopy radii, usually approximated by a power-law function at transverse momenta above 200 MeV/c. However, the radii behavior has been much less explored for the ultrasoft pions, possessing transverse momentum comparable to or lower than the pion mass. For many experimental setups this region is difficult to measure. In this work we present theoretical calculations of pion emission in the ultrasoft region in the two hybrid models iHKM and LHYQUID+THERMINATOR2. Along with the particle transverse momentum spectra, we present the calculated femtoscopy radii, in both one-dimensional and three-dimensional representations. We investigate the radii dependence on pair m_T and observe, in particular, a departure from the power-law behavior at ultrasoft momenta, potentially reflecting a decoupling of such slow pions from the rest of collectively expanding system. We provide the theoretical interpretation of this result and discuss its significance, in particular, for the ongoing nonidentical particle femtoscopy analysis for pairs consisting of a pion and a baryon (or of a pion and a charmed meson).

DOI: 10.1103/PhysRevC.110.034904

I. INTRODUCTION

The interferometry of particles emitted from small radiating source enables one to study the evolving geometry of that source. The particle interferometry originated from the experimental paper [1] and theoretical works [2,3]. In the latter it was also found that the results for the quantum statistics correlation effect for two close sources of identical particle emission in collision physics are formally similar to those for classical intensity correlations of the light radiation coming from different parts of a star, known in astronomy as the Hanbury-Brown–Twiss (HBT) effect [4–6]. The similarity, as well as the difference between the quantum correlations in identical-particle pairs and the classical HBT effect are analyzed, e.g., in [7]. Note that the correlation femtoscopy method, initially developed for finding the overall *size* of identical quantum particles' source, now is considered to measure the *homogeneity lengths* [8] of such femtometer -small sources. This general interpretation is especially important for the studies of the space-time structure of expanding sources, such as those created in proton/antiproton and heavy-ion collisions [1–3,9–14].

The homogeneity lengths, defined as a result of correlation femtoscopy analysis, reflect the spatial dimensions of the region within the entire strongly interacting system formed in the collision, from which particles are emitted with similar velocities (having close, nearly coinciding values and directions) [8,15]. Gaussian parametrizations for the particle emission source function (SF) and the two-particle correlation function (CF) are usually used in femtoscopy studies, although the realistic source shape differs from a perfect Gaussian; e.g., resonance decay contributions cause exponential behavior near the peak of the correlation function. The conventional use of the Gaussian shape allows one to standardize the description of experimental data and easily compare the results of different femtoscopy measurements, as well as to interpret the obtained radii as the homogeneity lengths. It is also well motivated experimentally in heavy-ion collisions, where correlation shapes for pions in three-dimensional (3D) analyses are universally observed to be Gaussian in a wide range of centralities and pair transverse momenta. The study of the dependence of the radii on the particle species, collision type, and collision energy is the main objective of the femtoscopic analysis of heavy-ion collisions.

In experimental studies, one clearly observes certain types of universal scaling behavior for the measured femtoscopy scales. For a given colliding system and collision energy a linear scaling of the femtoscopic radii is universally observed versus the cube root of the final state mean particle multiplicity, $\langle dN_{ch}/d\eta\rangle^{1/3}$ [16–22]. A similar scaling across collision energies and colliding systems is only approximate [23,24]. The radii versus the pair transverse momentum exhibit a power-law-like scaling in pair transverse mass m_T ($m_T = \sqrt{k_T^2 + m^2}$, where k_T is pair mean transverse momentum, $k_T = |\mathbf{p}_{T1} + \mathbf{p}_{T2}|/2$, and m is particle mass) [16,17,25–30].

In heavy-ion collisions both these scalings are predicted by hydrodynamic models [31,32]. Specifically, the m_T scaling is explained as a direct consequence and one of the main signatures of the collective radial flow of the system.

The observed m_T power-law scaling means a decrease of the radii with growing m_T that is a signature of hydrodynamic collectivity, typical for all particle species affected by the same flow field. Such dependence can be helpful for the prediction of the source size at certain m_T through the interpolation between radii measured at different m_T values. Nonetheless, the m_T range of experimental radii measurement depends on the acceptance of the detectors used in the study, and the very-low-m_T region has not been reached yet via such measurements. Therefore, the femtoscopy -scale predictions in that region can come only from extrapolation, which, following the commonly used power-law function, shows a very rapid growth of the radii with decreasing m_T. The theoretical studies, by contrast, do not face such problems, and so simulations within a realistic collision model can help estimate the possible character of the femtoscopy radii behavior in the ultrasoft momentum region.

The knowledge of femtoscopic radii for ultrasoft pions is becoming increasingly important in the context of rapidly developing experimental analyses of femtoscopic correlations of nonidentical particles [33,34]. In the case of such pairs the correlation occurs between two particles with similar velocity. If the pair in question contains a pion and a relatively massive particle (e.g., a deuteron or a charmed meson), then the pion in the pair needs to be ultrasoft in order to be correlated. The femtoscopic radius of the pair is directly related to the size of emission regions of both particles in the pair. Therefore, in order to study the non-identical correlations between pions and massive particles, the knowledge of femtoscopic radii of ultrasoft pions becomes essential.

Several previous theoretical studies of ultralow momentum pions were motivated by the experimental evidence of enhanced production [35,36]. These observations could be addressed by nonequilibrium models [37]. In addition to the semiclassical models, pure quantum effects such as pion condensation and Bose-Einstein enhancement were also explored [38]. However, none of these studies addressed the pion femtoscopic radii nor their scaling at very low transverse momenta.

Thus, in this paper, we focus on studying the pion femtoscopic radii dependence on pair m_T, including the region of very low transverse masses, in Pb-Pb collisions at the Large Hadron Collider (LHC) energy $\sqrt{s_{NN}} = 5.02$ TeV simulated within the integrated hydrokinetic Model (iHKM) [31,39,40] and the hydrodynamics model [41] coupled to the statistical hadronization code THERMINATOR2 (LHYQUID + THERMINATOR2) [42]: LQTH.

II. MODELS' DESCRIPTION

The collisions of heavy ions at ultrarelativistic energies allow to create quark-gluon plasma (QGP): a new state of strongly interacting matter, where quarks and gluons are no longer confined within individual nucleons. The evolution of such matter can be successfully described in complicated models realized in the form of codes for labor-consuming computer simulations. Such codes typically include modules describing the initial state formation, relativistic hydrodynamics expansion of liquid-like QGP at the intermediate stage of the system's evolution, its subsequent particlization (turning into a set of hadrons), and, finally, the hadron-resonance gas expansion. As a result of typical calculation, one obtains from the model a set of created hadrons, characterized by the space-time points of their last collision and four-momenta. Based on these data one can construct different observables, like spectra, correlation functions, etc.

The data analyzed in this study were generated using two such models, iHKM and LQTH, each having its own characteristics.

The iHKM is one of the most complete models, describing all the essential phases of the matter evolution in the course of a relativistic $A + A$ collision (see [31,39] for details). The initial conditions (ICs) for each simulation include the energy density spatial distribution at the starting time τ_0, usually close to 0.1 fm/c (for the high-energy collisions we use GLISSANDO code [43] to generate it), and anisotropic momentum distribution, inspired by the color glass condensate model. These ICs correspond to the very initial nonequilibrium partonic state right after the two nuclei collision. At the next stage of the system's evolution, it gradually thermalizes and approaches a nearly hydrodynamical state. Then (starting from the thermalization time $\tau_{\rm th} \approx 1$ fm/c) there follows a continuous medium expansion described in the Israel-Stewart viscous hydrodynamics formalism. As the matter expands and cools down, it eventually reaches the "particlization temperature" $T_p \approx 160$ MeV (depending on the QGP equation of state used at the hydrodynamics stage), when one switches to the description of the system in terms of hadrons (here the Cornelius routine [44] is applied). Produced hadrons are then fed to the UrQMD hadron cascade code [45,46], performing multiple hadronic rescatterings and resonance decays taking place at this final "afterburner" phase of the collision. The model is calibrated based on the experimental mean charged particle multiplicity and pion p_T spectrum slope in the most central collisions of a given type. In this paper, we use the iHKM tuning, used for the LHC 5.02 ATeV Pb-Pb collisions simulation described in detail in [40].

The LQTH is similarly properly calibrated to describe the $\sqrt{s_{NN}} = 5.02$ TeV Pb-Pb collisions at the LHC. The model assumes a second order viscous (3+1)D hydrodynamics evolution of the created fireball including shear and bulk viscosity as well as the Israel-Stewart stress corrections. The hydrodynamic expansion starts at 0.6 fm/c and lasts until the single (both chemical and kinetic) freeze-out at a selected temperature ($T_p \approx 140$ MeV), where statistical hadronization takes place. The system's chemical composition and momentum spectra no longer change, except for the resonance propagation and decays, which are simulated by the THERMINATOR2 package. At the freeze-out temperature, particles are generated according to statistical rules from the freeze-out hypersurface following the Cooper-Frye formula. The model reproduces the heavy-ion collisions results including flow and femtoscopic measurements [32,41,47]. All details about the

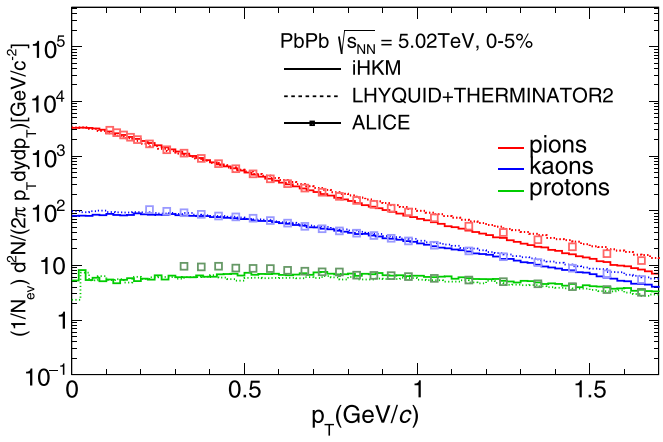

FIG. 1. Pion, kaon, and proton transverse momentum spectra calculated in the iHKM (solid lines) and in the LQTH models (dashed lines) for the most central $\sqrt{s_{NN}} = 5.02$ TeV Pb-Pb collisions at the LHC [48].

model implementation and initial conditions can be found in [41].

Both models describe well the experimental results for pion, kaon, and proton transverse momentum spectra, including the region of very soft momenta (see Fig. 1). Note, that such a description is achieved without the implementation of additional specific mechanisms of the soft pion emission, like the Bose-Einstein condensation, discussed, e.g., in [38]. Also, the two utilized models were previously used to successfully describe the LHC data on 2.76 ATeV Pb-Pb collisions [32,39,40,47].

III. CONSTRUCTION OF THE CORRELATION FUNCTION

The femtoscopic radii constituting the main subject of this study are typically defined from the Gaussian fits to the correlation functions depending on pair relative momentum $q = p_1 - p_2$. Here we consider the correlations in pairs of identical charged pions (π^+ and π^-), performing 1D and 3D analysis. The 1D correlation of identical particles is calculated as a function of $q_{\rm inv} = \sqrt{q_0^2 - \mathbf{q}^2}$ in the pair rest frame (PRF) and requires minimal statistics in contrast to the 3D study. However, the radius $R_{\rm inv}$, in this case, is the only length extracted, so that the emission source is assumed to be a spherically symmetric Gaussian one. The 3D study is based on relative momentum components $q_{\rm out}$, $q_{\rm side}$, and $q_{\rm long}$ calculated in the longitudinally comoving system (LCMS), where the longitudinal direction is along the beam axis, the outward direction is along the pair transverse momentum and the sideward direction is perpendicular to the other two. Accordingly, the three radii $R_{\rm out}$, $R_{\rm side}$, and $R_{\rm long}$ are extracted from the CF fit in this case.

The correlation function is generally defined as

$$C(p_1, p_2) = \frac{P_{12}(p_1, p_2)}{P_1(p_1)P_2(p_2)}, \tag{1}$$

and can be understood as the ratio of conditional probability to detect a pair of particles with the specific momentum values, $P_{12}(p_1, p_2)$, to the probability of finding them with such momenta independently, $P_1(p_1)P_2(p_2)$.

In experimental analysis, the procedure of obtaining the correlation function is based on making pairs of detected particles. One uses particles coming from the same event to build the correlated distribution (numerator), while for the background distribution (denominator) pairs are created using particles coming from different events (meaning that they retain all aspects of experimental acceptance, while not being correlated due to the mutual interaction).

In simulation studies, one usually fills two histograms (1D or 3D, depending on the analysis type) representing the corresponding particle pairs' relative momentum q distribution—one histogram for the numerator and another one for the denominator in Eq. (1)—based on the generated model output (set of hadrons). However, since in all currently available heavy-ion collision models the quantum statistical effects (including the Bose-Einstein symmetrization of the two identical bosons' wave function) are not implemented directly, on a microscopic level, one usually introduces a weight factor

$$w = 1 + \cos(qr), \tag{2}$$

coming from the Bose-Einstein interference at the so-called "afterburner" stage (to simplify the presentation, Coulomb and strong final-state interactions are not considered here). This factor w is taken as a weight for the pairs entering the correlated distribution histogram (a numerator one). For the background distribution (denominator) the weight is equal to 1. In this study, we also use the rapidity cut, $|y| < 1$, during the identical charged pion pairs selection to reproduce the acceptance of the ALICE detector.

To obtain a fitting formula for the CF, which will allow us to define the desired femtoscopy radii, one can consider the 7D (if particles are on the mass shell) particle emission functions $S_i(x, p)$ for each particle species i and derive the approximate expressions for single-particle and two-particle momentum spectra, and then using Eq. (1) obtain the well known Bertsch-Pratt [49,50] representation for the correlation function of two identical bosons in LCMS:

$$C(\mathbf{k}, \mathbf{q}) = 1 + \lambda_{\rm 3D}(\mathbf{k}) \exp\big(- R^2_{\rm out}(\mathbf{k}) q^2_{\rm out} - R^2_{\rm side}(\mathbf{k}) q^2_{\rm side} - R^2_{\rm long}(\mathbf{k}) q^2_{\rm long} \big), \tag{3}$$

where femtoscopic radii R_i depend on mean pair momenta $\mathbf{k}$, and $\lambda_{\rm 3D}$ are referred to as correlation strength factors.

The invariant one-dimensional form of the correlation function Gaussian parametrization is

$$C(k, q_{\rm inv}) = 1 + \lambda_{\rm 1D}(k) \exp\big(- R^2_{\rm inv}(k) q^2_{\rm inv} \big). \tag{4}$$

IV. PION FEMTOSCOPY SCALES

This section presents the results on pion femtoscopic radii obtained as a result of correlation function fitting for identical pions in 1D and 3D studies using the two models (iHKM and LQTH). The correlation functions were calculated separately for the six centrality classes (0–5%, 5–10%, 10–20%, 20–30%, 30–40% and 40–50%) and the ten k_T ranges (0.00–0.05, 0.05–0.10, 0.10–0.15, 0.15–0.20,

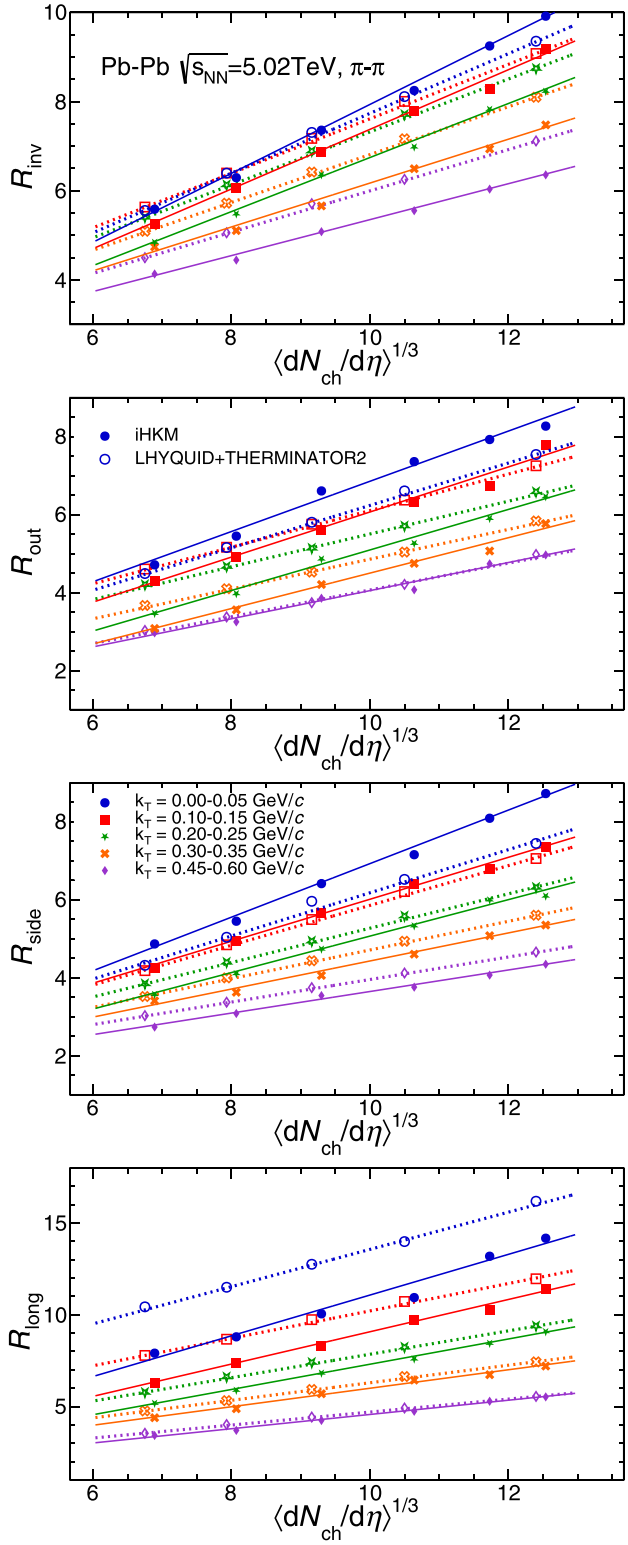

FIG. 2. Femtoscopic radii of charged identical pions as functions of $\langle dN_{ch}/d\eta \rangle^{1/3}$ calculated using iHKM (full markers) and LQTH (empty markers) models, for five k_T ranges (from top to bottom: 0.00–0.05, 0.10–0.15, 0.20–0.25, 0.30–0.35, 0.45–0.60 GeV/c). Different panels from top to bottom correspond to 1D R_{inv} and 3D R_{out}, R_{side}, and R_{long} radii respectively. Lines correspond to linear fits to the radii dependencies. Symbols are slightly shifted in the x direction for visibility.

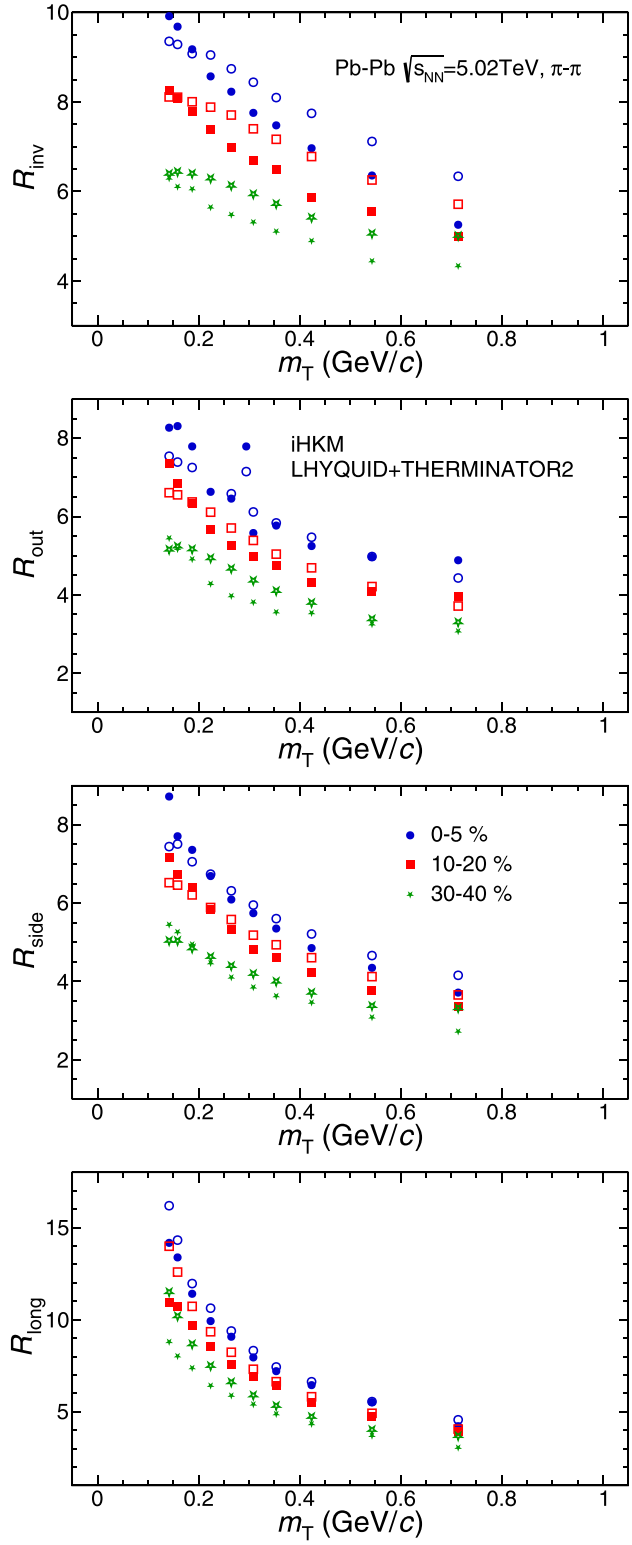

FIG. 3. Femtoscopic radii of charged identical pions as functions of m_T calculated using iHKM (full markers) and LQTH (empty markers) models, for the three centrality classes (0–5% blue, 10–20% red, 30–40% green). Different panels from top to bottom correspond to 1D R_{inv} and 3D R_{out}, R_{side}, and R_{long} radii respectively.

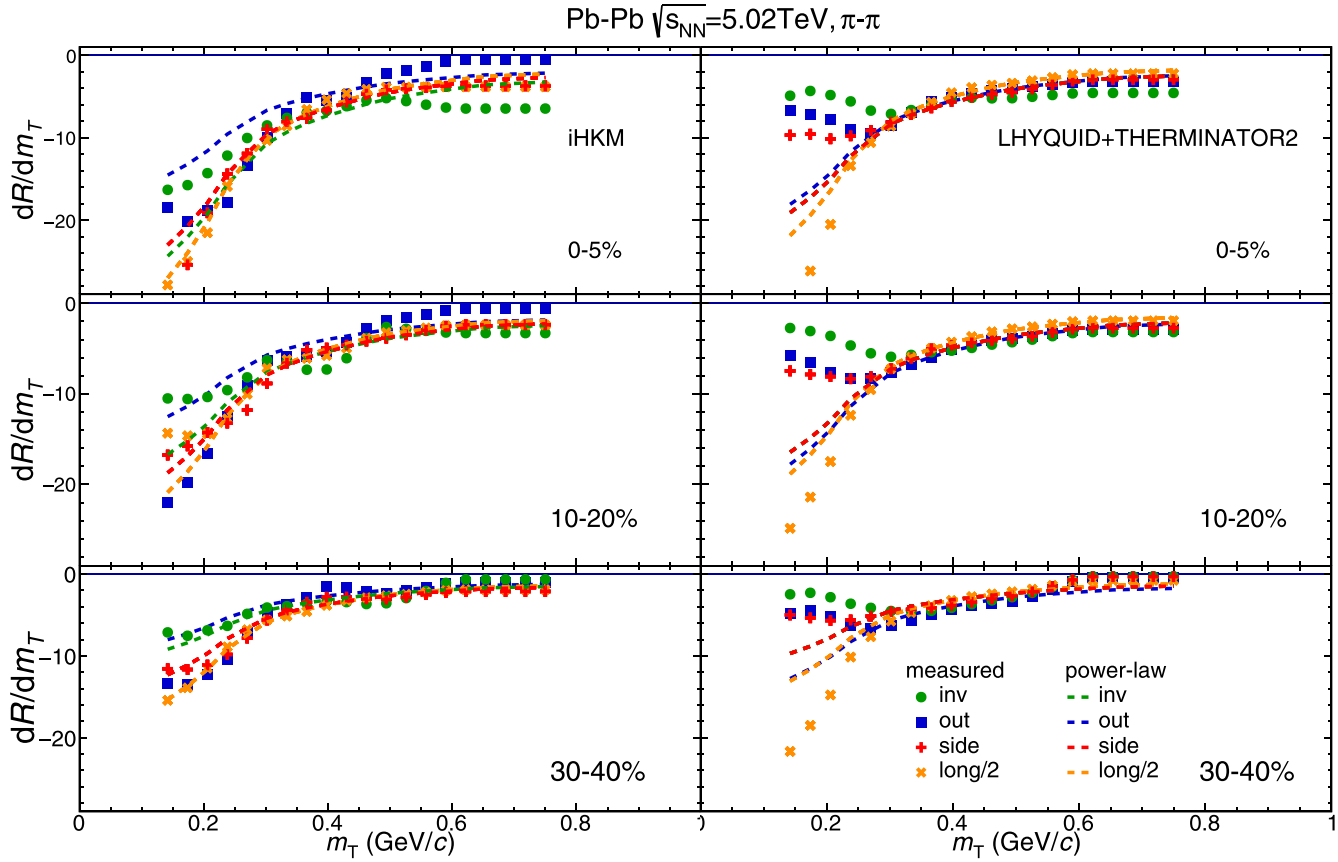

FIG. 4. First-order derivative of the charged identical pions' femtoscopic radii m_T dependency, dR/dm_T, in the iHKM (left) and the LQTH (right) models, for the three collision centralities (from top to bottom: 0–5%, 10–20%, 30–40%). Each panel contains derivatives of the three radii from the 3D study ($R_{\rm out}$ blue, $R_{\rm side}$ red, $R_{\rm long}$ orange) and $R_{\rm inv}$ from the 1D study (green). Markers represent results obtained from simulations and the dashed lines are obtained for the expected power-low trend based on fits to simulation points above 250 MeV/c.

0.20–0.25, 0.25–0.30, 0.30–0.35, 0.35–0.45, 0.45–0.60, 0.60–0.80) GeV/c. The results from both models were based on approximately 2×10^5 events, and the statistical uncertainty of each correlation function was much smaller than the systematic effects.

In Fig. 2 all the radii for identical pion pairs, corresponding to 1D and 3D calculations in the two models are demonstrated as functions of $\langle dN_{ch}/d\eta \rangle^{1/3}$. The results for five of all ten m_T bins are shown for better visibility since the radii in all bins follow a monotonic trend. The radii values vary in the range from about 15 fm ($R_{\rm long}$ for the lowest m_T and the highest multiplicity in LQTH) to about 2 fm ($R_{\rm side}$ for high m_T and low multiplicity in iHKM). All the radii universally grow linearly with the cube root of final-state multiplicity. The multiplicity dependencies for various m_T ranges generally show m_T ordering, except for 1D and transverse 3D results from the LQTH model, where the first bins of m_T overlap. This is because, in the LQTH model, radii of the first m_T bins take similar values. Figure 3, where femtoscopic radii are shown as functions of m_T presents it more clearly. All the measured radii decrease with increasing m_T. However, in the case of the LQTH model, we can observe a small plateau for the 1D and the transverse 3D radii at low m_T. The iHKM results, however, mostly fall monotonically in the lowest m_T region. Figure 3 also exhibits an expected ordering with respect to analysed centrality: the more peripheral the collision, the smaller the radii. In both Figs. 2 and 3, the difference in femtoscopy scales between the two models is also evident.

One can see from Fig. 3 that the femtoscopic radii in the iHKM model decrease faster than in the LQTH one. This is likely due to a very early, at $\tau_0 = 0.1$ fm/c, expansion start in the iHKM, leading to stronger velocity gradients at the final stage. This is the main reason for the reduction of the femtoscopic radii: the homogeneity lengths are reduced with the growing flow intensity. So, at the intermediate and high k_T the iHKM radii are smaller than those in the LQTH model with a later start of the expansion ($\tau_0 \approx 0.6$ fm/c). For the radii values at ultrasoft transverse momenta, the situation becomes even more complicated. At very small k_T the transverse radii are larger in the iHKM approach (the mentioned gradient could be the reason), while the longitudinal ones are larger in the LQTH model. The physics of pion production in the very-low-k_T region appears to be nontrivial and worthy of further study and better understanding.

To better investigate the character of the radii $m_{\rm T}$ dependencies, they were differentiated, and the obtained derivatives are presented in Fig. 4 (for the three centrality classes). The derivative has been extracted in the range ± 0.07 GeV/c around each point in the figure. Most of the functions show

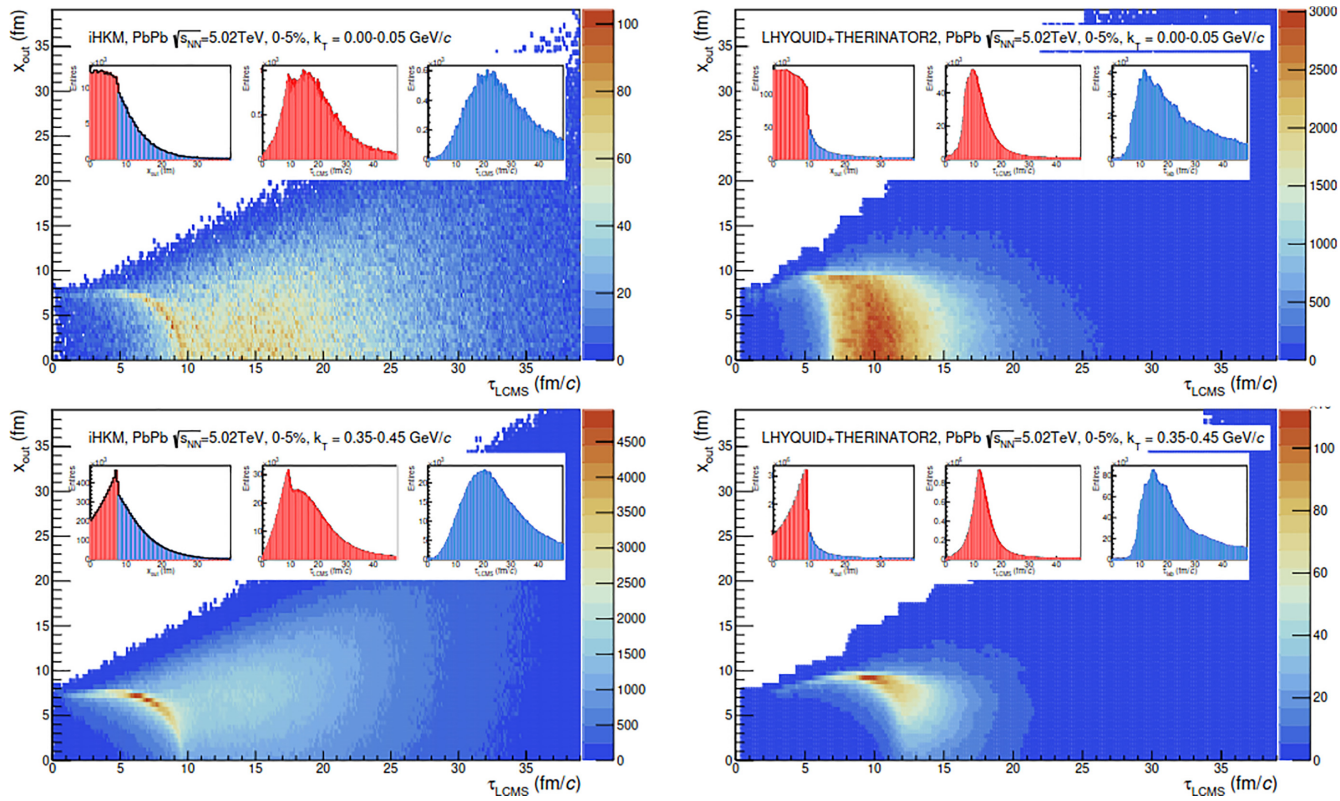

FIG. 5. The pion last interaction time and transverse coordinate in the out direction of the LCMS system for iHKM (left) and LQTH (right) simulations of Pb-Pb $\sqrt{s_{NN}} = 5.02$ TeV collisions. The upper panels show distributions for the lowest k_T interval, and the bottom ones show distributions for the middle k_T interval considered in this study. Subfigures show projection on the x_{out} direction (left) and projection on the time axis for the two x_{out} ranges (center and right).

similar behavior, with a clear change in the derivative form at certain momenta. Namely, the derivative behavior at low momenta ($m_T < 0.25$ GeV$/c$), especially for the R_{out} and R_{inv} radii in LQTH model, is noticeably different from that of a power-law function derivative, typical for the higher momentum region and approximately followed even at low m_T by the dR_{long}/dm_T dependencies. In more detail, in the iHKM one observes that the radius derivatives for the 1D case go flatter and are smaller in absolute value than the R_{long} derivatives for all the collision centralities, while the *out* and the *side* curves go either slightly higher or slightly lower than the *long* one, depending on the collision type. In the LQTH model we see a somewhat different situation, but one rather similar for all the centrality classes: all the derivatives, except for the *long* one, at low m_T have much smaller absolute values than the power-law function and demonstrate nearly flat behavior with small falls and rises, so that the radii dependency in this region can be sufficiently well approximated by a linear function.

To interpret above mentioned results, one can use a very recent iHKM femtoscopy analysis [51] as follows. When the system has just formed (at times near 0.1 fm$/c$), huge gradients of density in the transverse direction take place, since the system is essentially finite and borders with vacuum. The gradient is not equal locally along the radial directions: it is stronger at the periphery and less strong in the center, where soft hadrons mostly come from. In the vicinity of the geometrical center of the system, its decay into free particles happens at significantly later proper times than for most other parts of the system. Such a difference in proper times of spectra formation can be up to 5 fm$/c$ [51]. Thus, in the context of the present study, one can expect that maximal formation times (about 15 fm$/c$) should be typical for the ultrasoft pions with transverse momenta less than 0.3 GeV$/c$, that are emitted from the central region of the fireball. For the pions radiated from other parts of the decaying expanding system and having higher transverse momenta, 0.45–2 GeV$/c$, the (proper) time of maximal emission is close to 10 fm$/c$ [51]. The situation looks like a pion trap formed in the center of the created quark-gluon–hadron system. The hadrons stay together (cannot leave the system) for a longer time in the system's center because of the following:

(i) very low (close to zero) transverse collective velocity;
(ii) smaller density gradient in the center during almost the entire duration of the evolution, as compared to noncentral and periphery parts;
(iii) the initially highest density in the geometrical center in central and semicentral nucleus-nucleus collisions. Therefore, for this high-mass-density region, it is difficult to expand because of the relatively small transverse pressure gradient in the center.

Note that we see the mentioned effects of non-power-law transverse radii behavior in the ultrasoft momentum region in

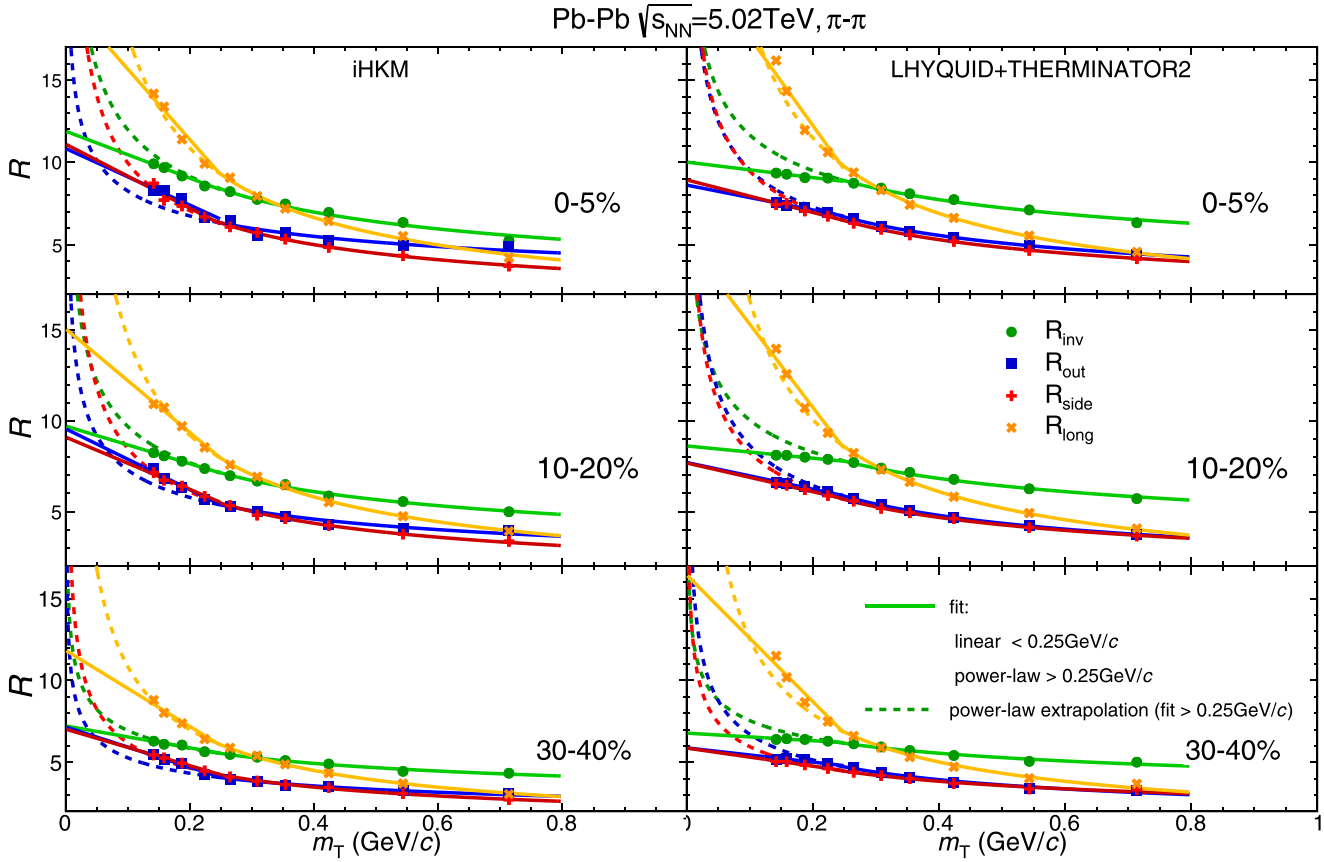

FIG. 6. Pion femtoscopic radii dependencies on m_T calculated in iHKM (left) and LQTH (right) models, for the three centrality classes (from top to bottom: 0–5%, 10–20%, 30–40%). Each panel contains results for the three radii from the 3D study ($R_{\rm out}$ squares, $R_{\rm side}$ crosses, $R_{\rm long}$ tilted crosses) and for $R_{\rm inv}$ from the 1D study (cicles). Lines correspond to power-law fits am_T^{-b} to radii dependencies in the range above 0.25 GeV/c.

"hydro plus hadronic cascade" models, where the dynamics is built in a quasiclassical approximation. The Bose-Einstein quantum statistics effect is taken into account in the very final stage only, but even this way, using the femtoscopy method, one can see specific (delayed freeze-out) features of emission in the ultra-low-momentum region (see also Fig. 1 from [51]). In particular, as we already mentioned, the femtoscopy analysis brings us the signal about formation of a long-lived ultrasoft pion trap in the central part of the system created in ultrarelativistic heavy ion collision. To further check this signal, we built the distributions of the transverse *out* coordinate of pion last collision points vs its time in the LCMS system; see Fig. 5. It can be easily noticed that in both models the origin of particles forming low and high k_T pairs is qualitatively different. Low k_T pairs are mainly created of particles with low momenta most intensively emitted from the decaying system close to its center. To see this, one can compare the red part of the $x_{\rm out}$ distributions shown in the panels of Fig. 5 for low (top panels) and high (bottom panels) particle momenta, respectively. The red parts correspond to the emission coming from the hadronizing hydrodynamic tube itself, while the blue parts correspond to the emission at larger distances from the expanding hadron-resonance gas. The blue parts are rather similar at low and high momenta, while the red ones have a maximum in the center of the system for low momenta and at the periphery of the system for higher momenta. The red time distributions at low momenta have two maxima and larger mean emission time than those at high momenta having only one maximum near the system's particlization time. The blue time distributions are similar for the low and high momentum cases.

The dependencies of the radii on m_T, together with the power-law fits, are presented for the three centrality classes in Fig. 6. The fitting was performed outside the "non-power-law" region observed in Fig. 4 (above 0.25 GeV/c). As one can see from Fig. 6, the power-law function in the form $am_{\rm T}^{-b}$ works well for all the radii at not very low momenta, and in case of the *long* direction it describes even the ultrasoft region below 0.25 GeV/c. Other radii, especially the 1D ones, at very low momenta go below (in the iHKM sometimes above) the power-law fitting curve.

In Fig. 6 the fall of 1D radii is less prominent than the fall for radii from 3D studies. This can be connected with the shape of the respective correlation functions. The 1D functions are less Gaussian than the 3D functions, and therefore the fitting has to compensate for this by reducing the correlation strength parameter λ. The m_T dependencies of λ in the two applied models are shown in Fig. 7. In the low m_T region λ behaves similarly in both cases, whereas with growing m_T it tends to go down in the 1D case.

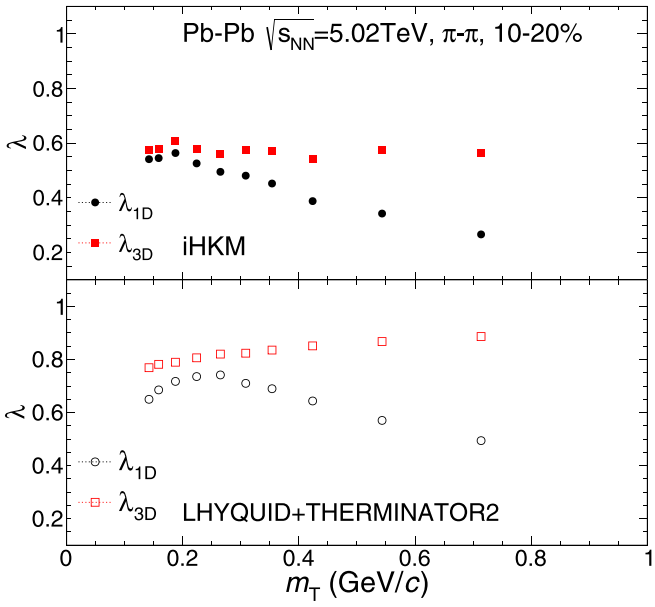

FIG. 7. The correlation strength λ parameters from 1D (black) and 3D (red) fits to the two-pion CF functions for the ten m_T bins. The iHKM (top) and the LQTH (bottom) results are shown for $c =$ 10–20% Pb-Pb collisions at $\sqrt{s_{NN}} = 5.02$ TeV.

Finally, we analyzed the femtoscopic-radii dependence on pair velocity; see Fig. 8 for different centrality intervals and for both used model approaches. In all cases, we notice a slow radii falling at low velocities. All the distributions were fitted with the analytic formula derived for the purpose of this study,

$$R(\beta) = \frac{a}{e^{(\beta-b)/c}+1}, \tag{5}$$

where $\beta = k_T/m_T$ is pair velocity, and a, b, c are free parameters of the fit. As particle velocity decreases, the radii seem to reach a saturated value, similar in a very broad range of β. Therefore such a value could be used to determine an extrapolated value of the radii for ultrasoft pions, instead of the historically used dependence based on power-law m_T scaling. It is particularly important for non-identical femtoscopy studies, where one considers pairs of particles with different masses moving at the same velocity, thus having different momenta.

V. SUMMARY

This paper presents a study of femtoscopic radii obtained from simulated data using iHKM and LQTH. The results point out that the power-law character of the femtoscopic m_T-caling is no longer valid for 1D studies in the low m_T region (below 250 MeV/c). In the case of 3D studies, the radii are better described by the power-law dependence than the 1D radii; however, the final conclusions are model dependent. The iHKM model results are closer to a power-law behavior, especially in the 3D analysis case. On the other hand, for the LQTH model one sees noticeable deviations from the power-law description everywhere, except for the longitudinal direction. Both models show that in low-m_T region radii distribution tends to be more linear than power law or even flat

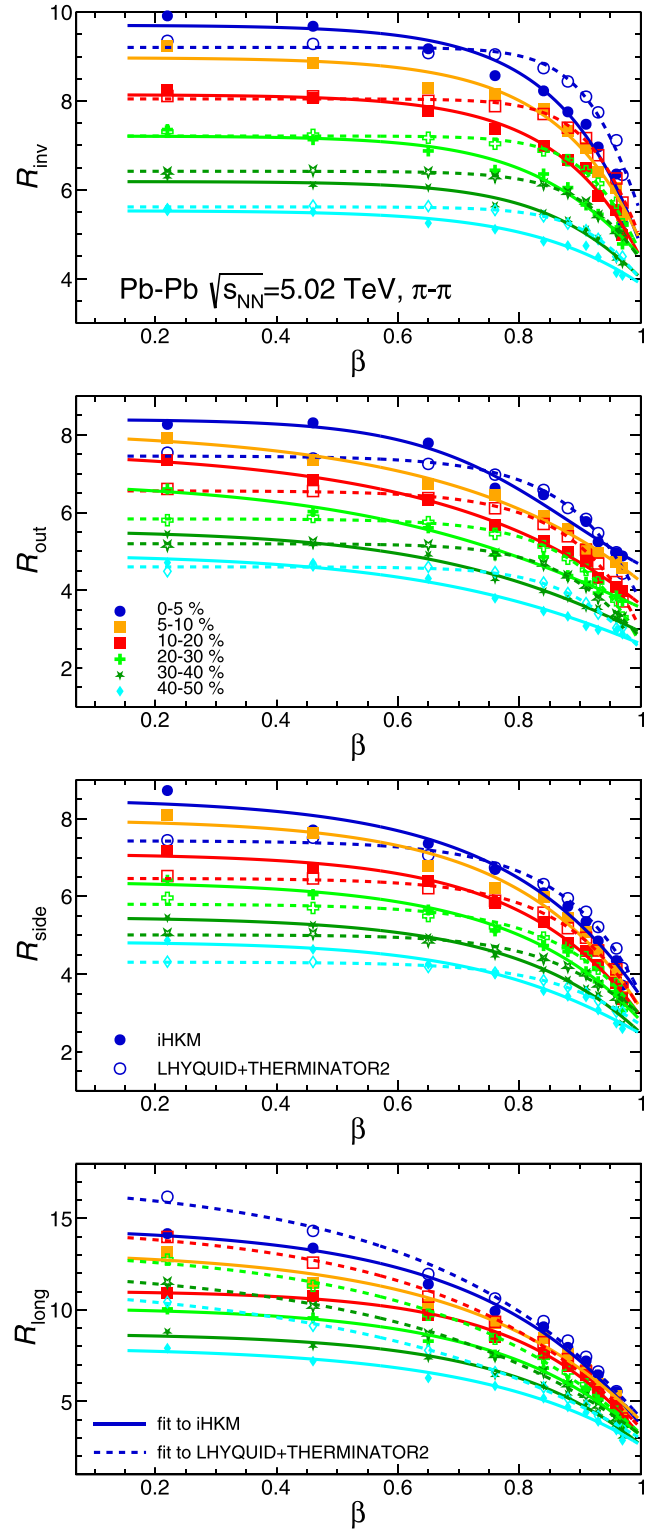

FIG. 8. The identical pion femtoscopy radii dependencies on pair velocity β in the iHKM (full markers) and the LQTH (empty markers) models. The results for the six centrality classes are shown. The lines represent fits to the radii by the formula (5).

in some cases. This results in smaller radii than expected from the extrapolation of the power-law scaling from intermediate and high m_T.

This modification of the behavior is motivated by the capacity of the ultrasoft pions to decouple from the energetic and dense core of the expanding system, resulting in longer emission times but from the center of the created system. This can be interpreted as both spatial and kinematic trapping of the ultrasoft pions by the more dense part of the created system. Such pions cannot escape this phase-space region until this confining mechanism is released. This finding is fundamental for addressing experimentally the expected pion radii in nonidentical femtoscopic studies when the second particle has a large mass difference with the pion mass, e.g., pion-deuteron, pion-omega, or pion-charm hadron pairs.

The observations of the non-monotonic behavior of ultrasoft pions obtained from semiclassical models should also be explored from the quantum perspective. The role of confinement and its connection to the direct photon puzzle [52–56] might as well influence the pion homogeneity lengths and should be studied further.

ACKNOWLEDGMENTS

This work is funded by the Research University – Excellence Initiative of Warsaw University of Technology via the strategic funds of the Priority Research Centre of High Energy Physics and Experimental Techniques, the IDUB POSTDOC program, the IDUB YOUNG-PW program, Scientific Council of the discipline grant program, and the Polish National Science Centre under Agreements No. 2022/45/B/ST2/02029 and No. 2023/49/N/ST2/03525. The work was also supported by a grant from the Simons Foundation (Grant No. 1290596, Yu.S. and V.S.).

[1] G. Goldhaber, S. Goldhaber, W. Lee, and A. Pais, Influence of Bose-Einstein statistics on the antiproton-proton annihilation process, Phys. Rev. **120**, 300 (1960).
[2] G. I. Kopylov and M. I. Podgoretsky, Correlations of identical particles emitted by highly excited nuclei, Sov. J. Nucl. Phys. **15**, 219 (1972).
[3] G. I. Kopylov, Like particle correlations as a tool to study the multiple production mechanism, Phys. Lett. B **50**, 472 (1974).
[4] R. H. Brown and R. Q. Twiss, LXXIV. A new type of interferometer for use in radio astronomy, London Edinburgh Dublin Philos. Mag. J. Sci. **45**, 663 (1954).
[5] R. Q. Twiss and R. Hanbury Brown, Correlation between photons in two coherent beams of light, Nature (London) **177**, 27 (1956).
[6] R. Q. Twiss, A. G. Little, and R. Hanbury Brown, Correlation between photons, in coherent beams of light, detected by a coincidence counting technique, Nature (London) **180**, 324 (1957).
[7] Yu. M. Sinyukov and V. M. Shapoval, Correlation femtoscopy of small systems, Phys. Rev. D **87**, 094024 (2013).
[8] S. V. Akkelin and Yu. M. Sinyukov, The HBT-interferometry of expanding sources, Phys. Lett. B **356**, 525 (1995).
[9] S. E. Koonin, Proton pictures of high-energy nuclear collisions, Phys. Lett. B **70**, 43 (1977).
[10] M. Gyulassy, S. K. Kauffmann, and L. W. Wilson, Pion interferometry of nuclear collisions. I. Theory, Phys. Rev. C **20**, 2267 (1979).
[11] W. A. Zajc, J. A. Bistirlich, R. R. Bossingham, H. R. Bowman, C. W. Clawson, K. M. Crowe, K. A. Frankel, J. G. Ingersoll, J. M. Kurck, C. J. Martoff *et al.*, Two-pion correlations in heavy ion collisions, Phys. Rev. C **29**, 2173 (1984).
[12] A. N. Makhlin and Yu. M. Sinyukov, The pion interferometry theory for the hydrodynamic stage of multiple processes, Yad. Fiz. **46**, 637 (1987).
[13] A. N. Makhlin and Yu. M. Sinyukov, Hydrodynamics of hadron matter under pion interferometric microscope, Z. Phys. C **39**, 69 (1988).
[14] H. U. Gersch, Coulomb final state interaction in identical boson interferometry, Z. Phys. A: At. Nucl. **327**, 115 (1987).
[15] Yu. M. Sinyukov, Spectra and correlations in locally equilibrium hadron and quark-gluon systems, Nucl. Phys. A **566**, 589 (1994).
[16] K. Aamodt, A. Abrahantes, D. Adamova, M. Aggarwal, G. Aglieri Rinella, A. Agocs, S. Salazar, Z. Ahammed, N. Ahmad, A. Masoodi *et al.* (ALICE Collaboration), Two-pion Bose-Einstein correlations in central Pb-Pb collisions at $\sqrt{s_{NN}} =$ 2.76 TeV, Phys. Lett. B **696**, 328 (2011).
[17] J. Adam, D. Adamová, M. M. Aggarwal, G. Aglieri Rinella, M. Agnello, N. Agrawal, Z. Ahammed, S. U. Ahn, I. Aimo, S. Aiola *et al.* (ALICE Collaboration), One-dimensional pion, kaon, and proton femtoscopy in Pb-Pb collisions at $\sqrt{s_{NN}} =$ 2.76 TeV, Phys. Rev. C **92**, 054908 (2015).
[18] K. Aamodt *et al.* (ALICE Collaboration), Two-pion Bose-Einstein correlations in pp collisions at $\sqrt{s} = 900$ GeV, Phys. Rev. D **82**, 052001 (2010).
[19] J. Adam *et al.* (ALICE Collaboration), Two-pion femtoscopy in p-Pb collisions at $\sqrt{s_{NN}} = 5.02$TeV, Phys. Rev. C **91**, 034906 (2015).
[20] K. Aamodt *et al.* (ALICE Collaboration), Femtoscopy of pp collisions at $\sqrt{s} = 0.9$ and 7 TeV at the LHC with two-pion Bose-Einstein correlations, Phys. Rev. D **84**, 112004 (2011).
[21] J. Adam *et al.* (ALICE Collaboration), Centrality dependence of pion freeze-out radii in Pb-Pb collisions at $\sqrt{s_{NN}} = 2.76$ TeV, Phys. Rev. C **93**, 024905 (2016).
[22] S. Acharya *et al.* (ALICE Collaboration), Pion-kaon femtoscopy and the lifetime of the hadronic phase in Pb–Pb collisions at $\sqrt{s_{\rm NN}} = 2.76$ TeV, Phys. Lett. B **813**, 136030 (2021).
[23] S. V. Akkelin and Yu. M. Sinyukov, Phase-space densities and effects of resonance decays in a hydrodynamic approach to heavy ion collisions, Phys. Rev. C **70**, 064901 (2004).
[24] V. M. Shapoval, P. Braun-Munzinger, Iu. A. Karpenko, and Yu. M. Sinyukov, Femtoscopic scales in p+p and p+Pb collisions in view of the uncertainty principle, Phys. Lett. B **725**, 139 (2013).
[25] C. Adler *et al.* (STAR Collaboration), Pion interferometry of $\sqrt{s_{NN}} = 130$ GeV Au+Au collisions at RHIC, Phys. Rev. Lett. **87**, 082301 (2001).
[26] S. S. Adler *et al.* (PHENIX Collaboration), Bose-Einstein correlations of charged Pion Pairs in Au + Au collisions at $\sqrt{s_{NN}} =$ 200 GeV, Phys. Rev. Lett. **93**, 152302 (2004).

[27] J. Adams *et al.* (STAR Collaboration), Pion interferometry in Au+Au collisions at $\sqrt{s_{NN}} = 200$ GeV, Phys. Rev. C **71**, 044906 (2005).

[28] M. A. Lisa, S. Pratt, R. Soltz, and U. Wiedemann, Femtoscopy in relativistic heavy ion collisions: Two decades of progress, Annu. Rev. Nucl. Part. Sci. **55**, 357 (2005).

[29] B. Abelev, M. Aggarwal, Z. Ahammed, B. Anderson, D. Arkhipkin, G. Averichev, J. Balewski, O. Barannikova, L. Barnby, J. Baudot *et al.* (STAR Collaboration), Pion interferometry in Au + Au and Cu + Cu collisions at $\sqrt{s_{NN}} = 62.4$ and 200 GeV, Phys. Rev. C **80**, 024905 (2009).

[30] S. Acharya, D. Adamová, A. Adler, J. Adolfsson, M. M. Aggarwal, G. Aglieri Rinella, M. Agnello, N. Agrawal, Z. Ahammed, S. Ahmad *et al.* (ALICE Collaboration), Search for a common baryon source in high-multiplicity pp collisions at the LHC, Phys. Lett. B **811**, 135849 (2020).

[31] V. Yu. Naboka, S. V. Akkelin, Iu. A. Karpenko, and Yu. M. Sinyukov, Initialization of hydrodynamics in relativistic heavy ion collisions with an energy-momentum transport model, Phys. Rev. C **91**, 014906 (2015).

[32] A. Kisiel, M. Gałażyn, and P. Bożek, Pion, kaon, and proton femtoscopy in Pb–Pb collisions at $\sqrt{s_{NN}} = 2.76$ TeV modeled in (3+1)D hydrodynamics, Phys. Rev. C **90**, 064914 (2014).

[33] R. Lednicky, Finite-size effects on two-particle production in continuous and discrete spectrum, Phys. Part. Nucl. **40**, 307 (2009).

[34] A. Kisiel, Nonidentical-particle femtoscopy at $\sqrt{s_{NN}} = 200$ GeV in hydrodynamics with statistical hadronization, Phys. Rev. C **81**, 064906 (2010).

[35] B. Abelev *et al.* (ALICE Collaboration), Pion, kaon, and proton production in central Pb-Pb collisions at $\sqrt{s_{NN}} = 2.76$ TeV, Phys. Rev. Lett. **109**, 252301 (2012).

[36] B. Abelev *et al.* (ALICE Collaboration), Centrality dependence of π, K, p production in Pb-Pb collisions at $\sqrt{s_{NN}} = 2.76$ TeV, Phys. Rev. C **88**, 044910 (2013).

[37] V. Begun, W. Florkowski, and M. Rybczynski, Explanation of hadron transverse-momentum spectra in heavy-ion collisions at $\sqrt{s_{NN}} = 2.76$ TeV within chemical non-equilibrium statistical hadronization model, Phys. Rev. C **90**, 014906 (2014).

[38] V. Begun and W. Florkowski, Bose-Einstein condensation of pions in heavy-ion collisions at the CERN Large Hadron Collider (LHC) energies, Phys. Rev. C **91**, 054909 (2015).

[39] V. Yu. Naboka, Iu. A. Karpenko, and Yu. M. Sinyukov, Thermalization, evolution, and observables at energies available at the CERN Large Hadron Collider in an integrated hydrokinetic model of $A + A$ collisions, Phys. Rev. C **93**, 024902 (2016).

[40] V. M. Shapoval and Yu. M. Sinyukov, Bulk observables in Pb + Pb collisions at $\sqrt{s_{NN}} = 5.02$TeV at the CERN Large Hadron Collider within the integrated hydrokinetic model, Phys. Rev. C **100**, 044905 (2019).

[41] P. Bożek and I. Wyskiel-Piekarska, Particle spectra in Pb-Pb collisions at $\sqrt{s_{NN}} = 2.76$TeV, Phys. Rev. C **85**, 064915 (2012).

[42] M. Chojnacki, A. Kisiel, W. Florkowski, and W. Broniowski, THERMINATOR 2: THERMal heavy IoN generATOR 2, Comput. Phys. Commun. **183**, 746 (2012).

[43] P. Bożek, W. Broniowski, M. Rybczynski, and G. Stefanek, GLISSANDO 3: GLauber initial-state simulation AND mOre..., ver. 3., Comput. Phys. Commun. **245**, 106850 (2019).

[44] P. Huovinen and H. Petersen, Particlization in hybrid models, Eur. Phys. J. A **48**, 171 (2012).

[45] S. A. Bass *et al.*, Microscopic models for ultrarelativistic heavy ion collisions, Prog. Part. Nucl. Phys. **41**, 255 (1998).

[46] M. Bleicher *et al.*, Relativistic hadron-hadron collisions in the ultra-relativistic quantum molecular dynamics model, J. Phys. G: Nucl. Part. Phys. **25**, 1859 (1999).

[47] A. Kisiel, Pion-kaon femtoscopy in Pb–Pb collisions at $\sqrt{s_{NN}} =$ 2.76 TeV modeled in (3+1)D hydrodynamics coupled to Therminator 2 and the effect of delayed kaon emission, Phys. Rev. C **98**, 044909 (2018).

[48] S. Acharya, D. Adamová, S. P. Adhya, A. Adler, J. Adolfsson, M. M. Aggarwal, G. Aglieri Rinella, M. Agnello, N. Agrawal *et al.* (ALICE Collaboration), Production of charged pions, kaons, and (anti)protons in Pb-Pb and inelastic pp collisions at $\sqrt{s_{NN}} = 5.02$ TeV, Phys. Rev. C **101**, 044907 (2020).

[49] S. Pratt, Pion interferometry of quark-gluon plasma, Phys. Rev. D **33**, 1314 (1986).

[50] G. Bertsch and G. E. Brown, Temporal development of the plasma phase transition, Phys. Rev. C **40**, 1830 (1989).

[51] Yu. M. Sinyukov, V. M. Shapoval, and M. D. Adzhymambetov, Space-time structure of particle emission and femtoscopy scales in ultrarelativistic heavy-ion collisions, Universe **9**, 433 (2023).

[52] J.-F. Paquet, C. Shen, G. S. Denicol, M. Luzum, B. Schenke, S. Jeon, and C. Gale, Production of photons in relativistic heavy-ion collisions, Phys. Rev. C **93**, 044906 (2016).

[53] A. Adare, S. Afanasiev, C. Aidala, N. Ajitanand, Y. Akiba, R. Akimoto, H. Al-Bataineh, H. Al-Ta'ani, J. Alexander, A. Angerami *et al.* (PHENIX Collaboration), Centrality dependence of low-momentum direct-photon production in Au+Au collisions at $\sqrt{s_{NN}} = 200$ GeV, Phys. Rev. C **91**, 064904 (2015).

[54] J. Adam, D. Adamová, M. M. Aggarwal, G. Aglieri Rinella, M. Agnello, N. Agrawal, Z. Ahammed, S. U. Ahn, S. Aiola, A. Akindinov *et al.* (ALICE Collaboration), Direct photon production in Pb–Pb collisions at $\sqrt{s_{NN}} = 2.76$ TeV, Phys. Lett. B **754**, 235 (2016).

[55] V. Yu. Naboka, Yu. M. Sinyukov, and G. M. Zinovjev, Photon spectra and anisotropic flow in heavy ion collisions at the top RHIC energy within the integrated hydrokinetic model with photon hadronization emission, Nucl. Phys. A **1000**, 121843 (2020).

[56] H. Fujii, K. Itakura, and C. Nonaka, Photon emission at hadronization, Nucl. Phys. A **967**, 704 (2017).